Strange metal from local quantum chaos

Daniel Ben-Zion and John McGreevy

Strange metal from local quantum chaos

Daniel Ben-Zion and John McGreevy

Department of Physics, University of California at San Diego, La Jolla, CA 92093, USA

Abstract

How to make a model of a non-Fermi-liquid metal with efficient current dissipation is a long-standing problem. Results from holographic duality suggest a framework where local critical fermionic degrees of freedom provide both a source of decoherence for the Landau quasiparticle, and a sink for its momentum. This leads us to study a Kondo lattice type model with SYK models in place of the spin impurities. We find evidence for a stable phase at intermediate couplings.

2018/03/02

Contents

1   Introduction

How to make a model of a metal which is not a Fermi liquid, both in terms of the single-electron physics and in terms of its transport properties, is a long-standing problem in theoretical physics. A general field-theoretic strategy to make a non-Fermi liquid metal (NFL) is to couple a Fermi surface to some other gapless degrees of freedom. If those modes are bosonic (such as gauge fields or fluctuations of an order parameter)[1], the coupling must be (at least) trilinear, schematically $\psi^\dagger \psi \phi$, and the Landau quasiparticle decays predominantly by emission of soft ϕ modes. This process does not change the current much; in such models, therefore, the transport lifetime is much longer than the single-particle lifetime. On the other hand, there seem to exist NFLs where the two timescales are comparable, and have the same temperature dependence. This suggests that there should be other ways to make a NFL.

Not long ago, some people [2, 3, 4, 5, 6] were desperate enough to make progress on this problem that they tried to use gauge/gravity duality: an exotic large-N conformal field theory with a dual description in terms of Einstein gravity in one higher dimension was subjected to a chemical potential for a global $\mathsf{U}(1)$ symmetry.[2] The retarded Green's function of local fermionic operators in the resulting state revealed a Fermi surface in momentum space, near which the self-energy behaved as a power-law in

---

[1] For a review of the large literature, see [1].

[2] For a more leisurely discussion of these issues, see also §5 of [7].

frequency:

$$G_\psi(\omega, k) \overset{\text{small } \omega}{\sim} \frac{1}{\omega - v_F k_\perp - \mathcal{G}(\omega)}$$

with $\mathcal{G}(\omega) \sim \omega^{2\nu}$, indicative of a non-Fermi liquid metal. The special case of $\nu \to 1/2$, where $\mathcal{G} \sim \omega \log \omega$, is the marginal Fermi liquid Green's function of [8].

In [5], the power-law behavior was traced the region of the extra-dimensional geometry near the black-hole horizon. With the benefit of some hindsight [5, 9], the key feature of the near-horizon geometry of the black hole in this construction is that it describes a $z = \infty$ fixed point: its fluctuations are power-law in frequency, and essentially[3] independent of momentum – they are localized critical excitations. Hence, when coupled to a Fermi surface, they are able to render incoherent the propagation of the quasiparticles, and at the same time absorb arbitrary amounts of their momentum. Therefore, in a model where the quasiparticle decay is dominated by scattering off these excitations, the transport lifetime will equal the single-particle lifetime, and the power law in the conductivity $\rho(T)$ will match that of the fermion self-energy, as in the marginal Fermi liquid phenomenology [8].

The holographic construction summarized above, or even its 'semi-holographic' reduction [5, 9], have the drawback that the description of the $z = \infty$ fixed point is in terms of a mysterious gravitational system, whose dynamics is only under control in a limit $N \to \infty$ with infinitely many degrees of freedom at each point in space. Corrections to this limit require one to confront quantum gravity, or at least the back-reaction of quantum effects on the geometry [11, 12]. It would be useful to replace the near-horizon $AdS_2 \times \mathbb{R}^2$ region of the geometry with a more tractable locally critical system.

Such local quantum criticality is a fascinating idea, whose realization is desirable also as a justification of dynamical mean field theory [13, 14]. Such a fixed point is roughly a critical theory at each point in space, and hence requires the participation of many degrees of freedom. As explained in [15, 16, 17, 18], this intuition can be made precise by studying the dependence of the density of states on the energy. Dimensional analysis requires

$$\frac{dn}{dE}(E) = e^{S_0}\delta(E) + e^{S_1}\frac{1}{E}.$$

The first term represents a groundstate entropy S_0 and violates the Third Law of Thermodynamics. The second term is not integrable and requires the appearance of a new energy scale which violates the $z = \infty$ scaling and, as a consequence of this argument, cannot be disentangled from the low energy physics. The holographic

---

[3]In fact, as emphasized in [10], in the holographic construction described above, there is a weak, analytic dependence on the momentum. The authors of [10] call this 'semi-local criticality'. This is a feature of the holographic strange metal construction that we will not reproduce.

construction is most naturally interpreted in the canonical ensemble, and at $T \ll \mu$ and leading order in N, gives an extensive entropy which remains nonzero at $T \to 0$, suggesting a violation of the Third Law and the associated instabilities. The low-energy fate of the construction is obscured since classical gravity requires $N \to \infty$ before $T/\mu \to 0$, and by the fact that the gravity construction involves many degrees of freedom besides the Fermi surface.

This discussion motivates the study of more accessible constructions of $z = \infty$ fixed points, to which one might couple a Fermi surface. With this in mind, we cannot avoid thinking about the SYK (Sachdev-Ye-Kitaev) model [19, 20, 21, 22], which is a solvable model of local quantum criticality, and which has many features in common with (dilaton) gravity in AdS_2 [23, 24, 21, 22]. For our purposes of destroying quasiparticles, we require a $z = \infty$ fixed point with fermion operators carrying a conserved $\mathsf{U}(1)$ charge. Such a generalization of the SYK model is provided in [22]:

$$H_{\text{SYK}} = \sum_{ijkl}^{N} J_{ijkl} \chi_i^\dagger \chi_j^\dagger \chi_k \chi_l \qquad \overline{J_{ijkl}} = 0, \ \overline{J_{ijkl}^2} = \frac{J^2}{2N^3} \quad . \tag{1.1}$$

Its low-energy physics should be similar to dilaton gravity plus electromagnetism in AdS_2.

A single SYK model has no notion of space, since each fermion talks to every other. Since we are interested in the effects of the $z = \infty$ fixed point on the physics of the Fermi surface, we must introduce some notion of locality. Therefore, we consider a lattice of SYK clusters, decoupled from each other at the outset. Depicting a single 'cluster' of complex fermions as , a 1d implementation of the model can be illustrated as follows:
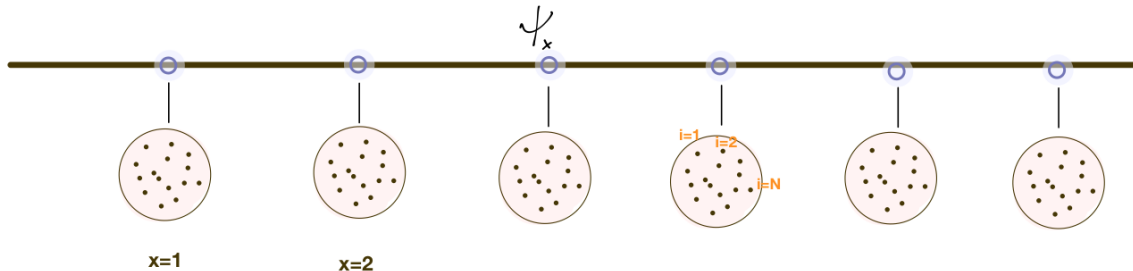

Figure 1: A cartoon of the model we study in this paper. Each blob represents an independent SYK model. The vertical edges represent the random couplings g_{ix}. The horizontal edges represent the translation-invariant hopping amplitudes t.

The model is a rather direct and crude discretization of the $AdS_2 \times \mathbb{R}^d$ near-horizon

3

geometry of the extremal charged black hole in AdS_{d+2}. Nevertheless, we will see that it reproduces many of the features of interest of the holographic strange metal of [5, 6].

To be specific, the hamiltonian we will study is $H = H_0 + H_{\text{int}}$, with

$$H_0 = -t \sum_{\langle xy \rangle \in \text{lattice}} \psi_x^\dagger \psi_y + h.c. + \sum_{x \in \text{lattice}} H_{SYK}(\chi_{xi}, J_{ijkl}^x), \quad H_{\text{int}} = \sum_{x,i} g_{ix} \psi_x^\dagger \chi_{xi} + h.c.$$

where ψ_x, χ_{xi} are complex canonical fermion annihilation operators, with $\{\psi_x^\dagger, \psi_y\} = \delta_{xy}$. Since ψ form a Fermi surface under H_0, we refer to them as itinerant fermions. We occasionally refer to the χ modes as cluster fermions. The couplings g_{ix} are independently Gaussian:

$$\overline{g_{ix}} = 0, \ \overline{g_{ix}g_{jy}} = \delta_{ij}\delta_{xy}g^2/N.$$

There are some precedents for our study. The result of hybridizing conduction electrons with the SY (as opposed to SYK) model, and its connection with holography, is studied in [23, 24]. The model studied in this paper is simpler in that no fractionalization is required to write down the Hamiltonian.

The system we study here has some similarities with models of heavy fermions, and in particular those devoted to understanding NFL behavior in those systems, such as, for example, [25]. This paper solves a model of conduction electrons coupled to localized f-electrons by random hybridization terms. The f-electrons have random site energies and a uniform Hubbard U. The model is approximated using dynamical mean field theory. There is a large literature studying such heavy-fermion-like models using DMFT. One goal of this work is to understand better the local (momentum-independent) form of the self-energy assumed by the DMFT analysis.

Some related work has also appeared during the overly long gestation of our project. [26] makes lattices of SYK clusters, coupled by a less dangerous four-fermion coupling, and studies the propagation of information. [27] studies the coupling of a single SYK cluster to fermions which can hop (essentially in infinite dimensions) by the same kind of hybridization term we study; this model lacks a notion of locality, however. [28] couples non-locally several flavors of SYK clusters. [29] studies the phase diagram of two clusters by quadratic terms. Most recently and closest to our work, [30, 31, 32] study a chain of SYK clusters coupled by (random and non-random) quadratic links; although the starting point does not have a Fermi surface, the resulting states of matter may be closely related to ours. Studies of higher-dimensional generalizations of the SYK model, with various motivations, include [33, 34, 35, 36, 37, 38, 39, 40]. In particular, [40] realizes a bosonic analog of the semi-holographic construction using SYK chains.

In the next section, we analyze the model at large N, arriving at the same picture as in the semi-holographic models. The advantage of having an explicit model of the

4

$z \to \infty$ fixed point is that we can analyze the extent to which the large-N and low-energy limits commute. In section §3, we analyze limits of the space of couplings and map out possible phase diagrams. In section §4, we attempt to make the fixed point perturbative by continuing in the number q of fermions participating in the SYK interactions. In section §5 we describe a DMRG study to decide between the possible phase diagrams proposed in §3.
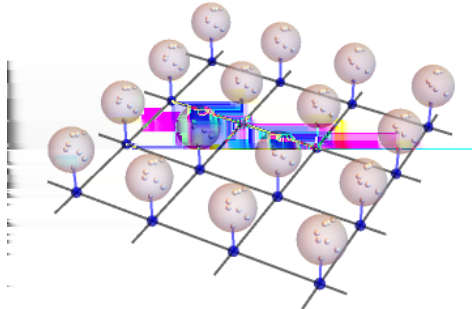

Figure 2: A diagram of the model in two spatial dimensions. The vertical (blue) bonds represent the random hybridization couplings g_{xi}. The black horizontal bonds are the uniform hoppings, t.

Most of our work applies in any number of spatial dimensions, and only the discussion of §5 is specific to one dimension. To emphasize this we include a diagram of the model in two dimensions in Fig. 2. In Fig. 3 we sketch our picture of the phase diagram of the model in the space of couplings $J/t, g/t$ studied here.

2 Large-N analysis

2.1 SYK review

We will use the complex fermion avatar of the SYK model described in [22], and here we provide a brief description of its relevant known properties. The degrees of freedom are a set of canonical fermions χ_i ($\{\chi_i, \chi_j^\dagger\} = \delta_{ij}, \{\chi_i, \chi_j\} = 0, i = 1..N$) governed by the Hamiltonian (1.1). The object of interest to us is the disorder averaged fermion green function $\mathcal{G}(\tau - \tau') = \overline{\left\langle \chi_a^\dagger(\tau)\chi_a(\tau') \right\rangle}$. This quantity can be calculated diagramatically by noticing that the only diagrams which survive disorder averaging are the ones in which interaction vertices can be grouped into pairs with identical indices.

The diagrams contributing at leading order in $1/N$ are those in which the vertices
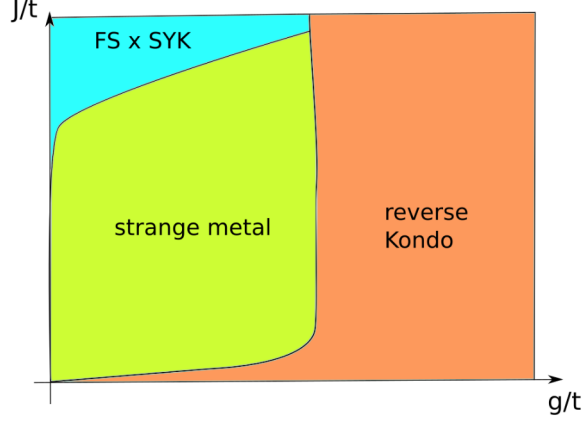
Figure 3: A (possibly optimistic) cartoon view of the proposed phase diagram. Orange: "reverse Kondo" refers to the regime where one linear combination of the fermions in each cluster hybridize with the mode of the Fermi surface at that site, leaving behind at low energies a chain of clusters with $N - 1$ modes. Even for large J, we expect that the hybridization term is a relevant perturbation of the SYK hamiltonian, so we expect this phase to continue into the upper right corner where t is the smallest energy scale. Cyan: When g/J is too small (at fixed N), the hybridization is unable to mix the levels of the clusters, and in the infrared, the Fermi surface decouples; this phase is labelled FS × SYK. We estimate this phase boundary to occur where g is comparable to the single-cluster level spacing: $g \sim \Delta E \sim e^{-aN} J$. At infinite N, therefore, this phase does not persist.

are paired as locally as possible starting from the interior of the diagram moving outwards: this leads to the series of so-called melon diagrams. This says that the one-particle irreducible part of $\mathcal{G}$, the self energy Σ, is itself a product of Green's functions: $\Sigma(\tau) = J^2 \mathcal{G}^2(\tau) \mathcal{G}(-\tau)$. Since there are no quadratic terms in H, the free propagator is $\mathcal{G}_0 = (\mathbf{i}\omega)^{-1}$ in frequency space.

At small frequencies and strong coupling, the free $(\mathbf{i}\omega)^{-1}$ part of Schwinger-Dyson equation for the fermion propagator $\mathcal{G}^{-1}(\omega) = (\mathbf{i}\omega)^{-1} - \Sigma(\omega)$ becomes negligible compared to the self energy, resulting in the following closed set of integral equations for the Green's function:

$$\int ds\, \mathcal{G}(\tau - s)\Sigma(s) \approx -\delta(\tau), \quad \Sigma(\tau) = J^2 \mathcal{G}(\tau)^2 \mathcal{G}(-\tau) = \quad \text{} .$$

These equations allow a power law solution for the Green's funciton; here we quote the result from [22]:

$$\mathcal{G}_{SYK}(\omega) = -\mathbf{i}\left(\frac{\pi}{J^2}\right)^{1/4} \sqrt{\frac{2\beta}{\pi}} \frac{\Gamma(\frac{1}{4} + \frac{\beta\omega}{2\pi})}{\Gamma(\frac{3}{4} + \frac{\beta\omega}{2\pi})}, \quad \mathcal{G}_{SYK}(\omega) = -\mathbf{i}\left(\frac{\pi}{J^2}\right)^{1/4} \frac{\operatorname{sgn}\omega}{\sqrt{|\omega|}}$$

6

at finite and zero temperature respectively, and at half filling. Away from half filling, the Green's function has a phase which we discuss in section 4. Most significantly, we note that the mass dimension of the SYK field is $\Delta(\chi(\tau)) = -\frac{1}{4}$.

We can consider generalizing the ($q = 4$)-fermion interactions of H_{SYK} to more general powers: $H(\chi) = J_{i_1 \cdots i_q} \chi_{i_1}^\dagger \cdots \chi_{i_q}$. Redoing the above analysis gives $\nu(q) = \frac{2-q}{2q}$ and mass dimension $\Delta_q(\chi(\tau)) = -\frac{1}{q}$. We will take advantage of this parameter in §4.

It is also possible to define - and consider coupling to - the *bath field*

$$\tilde{\chi}_i \equiv \sum_{jkl} J_{ijkl} \chi_j^\dagger \chi_k \chi_l$$

which is the object multiplying χ_i in H_{SYK}. The bath field has correlator and scaling dimension

$$\left\langle \tilde{\chi}^\dagger(\omega) \tilde{\chi}(\omega) \right\rangle \propto (\mathbf{i}\omega)^{+\frac{1}{2}}, \quad \Delta(\tilde{\chi}(t)) = \frac{3}{4}.$$

For general q, these are modified to $\left\langle \tilde{\chi}^\dagger(\omega) \tilde{\chi}(\omega) \right\rangle \propto (\mathbf{i}\omega)^{\frac{q-2}{q}}$ and $\Delta(\tilde{\chi}(t)) = \frac{q-1}{q}$.

2.2 Using SYK clusters to kill the quasiparticles and take their momentum

The system we will study for the rest of the paper has $H = H_{FS} + H_{SYK} + H_{\text{int}}$ with

$$H_{FS} = \sum_{\langle xy \rangle} t \psi_x^\dagger \psi_y + h.c. = \int d^d k \epsilon(k) \psi_k^\dagger \psi_k, \quad H_{\text{int}} = \sum_{x,i} g_{ix} \psi_x^\dagger \chi_{xi} + h.c.$$

We denote respectively the unperturbed and full $\langle \psi\psi \rangle$ propagators with a thin and thick black line. The $\langle \chi\chi \rangle$ propagator, denoted by a red line, includes the full series of melon diagrams. Disorder contractions are drawn as a dashed line.

$$\longrightarrow = \frac{1}{\omega - v_F k_\perp}, \qquad \textcolor{red}{\longrightarrow} = \left\langle \chi_x^\dagger \chi_y \right\rangle, \qquad \overset{\frown}{\diagup\diagdown} = \text{disorder contraction}$$

The itinerant-fermion Green's function is given by a series of alternating ψ and χ propagators. The only choice to make is how to contract the various interaction vertices in doing the Gaussian disorder averages. Any pattern other than the one shown below constrains an index sum over SYK flavors and is therefore suppressed by powers of $1/N$:

Thus, the ψ self-energy is $\Sigma(\omega, k) = g^2 \mathcal{G}(\omega)$ (just as in the holographic model). If we are interested in low energy physics near the Fermi surface, the SYK clusters are

in the conformal limit and the Green's function behaves as

$$G_\psi(\omega, k) \stackrel{\text{small } \omega}{=} \frac{1}{\omega - v_F k_\perp - g^2 \mathcal{G}_{SYK}(\omega)}$$

This is of the same form as found in the charged black hole calculation. In that context, various ν arise, but all have $\nu \geq 0$. In contrast, our model has $\nu = -\frac{1}{4}$, that is, $\mathcal{G}(\omega) \sim \omega^{-\frac{1}{2}}$. This self-energy is not only non-analytic, but also *infinite* at $\omega \to 0$. As a consequence, the Green's function *vanishes* at the Fermi surface. The spectral density $A(k, \omega) = \frac{1}{\pi} \text{Im} G(k, \omega)$ near the Fermi surface is illustrated in Fig. 4. For general q, the exponent is $2\nu = \frac{2}{q} - 1$, still negative for all $q > 2$.
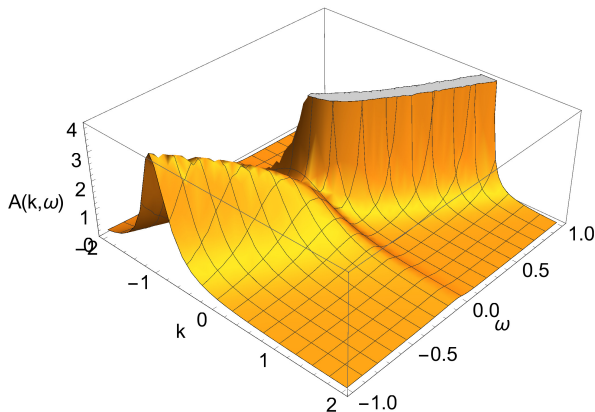

Figure 4: The self-energy diverges at $\omega = 0$, leading to a *zero* of the Green's function, and of the spectral density $A(k, \omega)$, exactly at the Fermi surface.

Coupling to the bath field $\tilde{\chi}$ would seem to give a more-familiar positive value of $\nu = +\frac{1}{4}$. For general q, it would give $\nu = \frac{q-2}{2q}$, which approaches a marginal fermi liquid as $q \to \infty$. We will see below, however, that this is a place where the $N \to \infty$ and low energy limits do not commute.

The conductivity from the itinerant fermions can be calculated using the Kubo formula. In the large N limit, the transport analysis of [41, 42] (and related semi-holographic analyses [43, 44]) can largely be carried over. The temperature dependence of the DC conductivity is a power-law determined by the localized-fermion Green's function exponent as $\sigma \propto T^{-2\nu}$. In particular, coupling to the SYK fermion and coupling to the bath field yield, at large N, a resistance which is proportional to $T^{-1/2}$ and $T^{1/2}$ respectively.

The divergence of the resistance as $T \to 0$ is related to the fact that the hybridization coupling is a relevant perturbation; this is a similar phenomenon to the resistance minimum in the Kondo problem [45]. In the Kondo case, the interaction is only marginally relevant, and hence the resistance minimum occurs at an exponentially low scale; here, for $q > 2$ the interaction is relevant by a finite amount. In the limit $q \to 2$, the interaction becomes marginal, suppressing the temperature at which the resistance rise sets in. We study this limit further in §4.

Does the Fermi surface delocalize the clusters?

Contributions to the cluster fermion Green's function $\mathcal{G}$ are again of the form

where the only decision to be made is the manner of disorder contraction. Here is a place where the randomness of the hybridization couplings g_{ix} is crucial: the processes by which $\mathcal{G}_{xy}$ would develop off-diagonal terms vanish by the disorder average over g_{ix}. The cluster fermions therefore stay localized, on average (however $\overline{\mathcal{G}_{xy}\mathcal{G}_{xy}}$ will not be zero).

Futhermore, the onsite corrections to the SYK Green's function are small; they are of order $1/N$. The leading order correction is obtained by summing the 'turtle' diagrams in Fig. 5. Taken together, this series of diagrams combines into the object $\frac{g^2}{N}\mathcal{G}_0^2(\omega) \int \mathrm{d}^d k \ G(k\omega)$, as we show in Appendix A. Thus there is the possibility that the SYK-ness of the cluster fermion will be disrupted at parametrically low energies. In Appendix A, we show that this correction in fact does not modify the leading low frequency behavior, even at frequencies small compared to $1/N$.
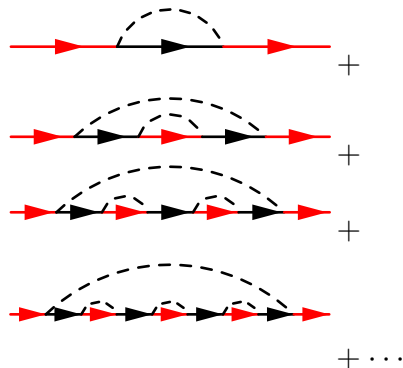

Figure 5: The corrections to the localized-fermion propagator $\mathcal{G}$ at order $1/N$.

Now consider the effects of $\delta\mathcal{G}$ on the itinerant propagator. The leading-in-N self-energy $\mathcal{G}(\omega)$ itself diverges like $\omega^{-1/2}$ at low frequency. It therefore dominates over $\delta\mathcal{G}$, which vanishes at asymptotically small ω, as we show in Appendix A.

2.3 Replica analysis

The leading-order diagrammatic calculation above can be reproduced by a replica calculation. It suffices to consider a single cluster impurity. The replicated action before

any disorder averaging is

$$S[\psi, c] = \sum_a \int d\tau \sum_i \bar{c}_{ia\tau} \partial_\tau c_{ia\tau} + \bar{f}_{xa\tau} (\partial_\tau - \xi(\partial_x)) f_{xa\tau}$$

$$+ \sum_{ijkl} J_{ijkl} \bar{c}_{ia\tau} \bar{c}_{ja\tau} c_{ka\tau} c_{la\tau} + \sum_i g_i \bar{c}_{ia\tau} f_{a\tau}(r_{imp}) + h.c.$$

Here $\xi(k)$ is the band dispersion. In what follows, we will occasionally drop the time arguments for compactness of writing. In that case the argument τ is always accompanies the replica index a and τ' with b. Averaging over gs with a gaussian weight of width g produces a term

$$\mathcal{I} \equiv \exp\left(\frac{g^2}{2N} \int d\tau d\tau' \bar{f}_a(r_{imp}, \tau) f_b(r_{imp}, \tau') \sum_i c_{a\tau i} \bar{c}_{b\tau' i}\right).$$

This is decoupled with two hermitian Hubbard Stratonovich (HS) fields $\rho_{ab}(\tau, \tau')$ and $\sigma_{ab}(\tau, \tau')$. By 'hermitian', we mean $\rho_{ab}(\tau, \tau') = \rho_{ba}^\star(\tau', \tau)$.

$$\mathcal{I} = \int D\rho_{ab} D\sigma_{ab} \exp\left[-\frac{1}{2} \int d\tau d\tau' \, N \sum_{ab} \rho_{ab}^2(\tau, \tau') + \sigma_{ab}^2(\tau, \tau') + \frac{1}{2} \int d\tau d\tau' g\left(\sum_{ab} \rho_{ab} F_{ab}^- + \mathbf{i}\sigma_{ab} F_{ab}^+\right)\right]$$

where $F_{ab}^\pm = \bar{\psi}_a(\tau)\psi_b(\tau') \pm \sum_i \bar{c}_{ia}(\tau)c_{ib}(\tau')$.

Introducing two sets of Hubbard-Stratonovich fields following Bray-Moore [46] and Sachdev [22], we can factorize the contribution from the average over J as

$$\int \prod_{ijkl} dJ_{ijkl} \, e^{-N^3 \frac{J_{ijkl}^2}{J^2}} e^{\int dt J_{ijkl} \bar{c}_i c_j \bar{c}_k c_l} = e^{\frac{J^2}{4N} \sum_{ab} \int dt \int dt' |\sum_i \bar{c}_{iat} c_{ibt'}|^4}$$

$$= \int [dQdP] \exp\left(\int d\tau d\tau' \sum_{ab} \left(-\frac{N}{4J^2} Q_{ab}(\tau, \tau')^2 - \frac{N}{2} Q_{ab} |P_{ab}(\tau, \tau')|^2 + Q_{ab} P_{ba} \sum_i \bar{c}_{ia} c_{ib}\right)\right)$$

$$\tag{2.1}$$

where Q and P are real and complex symmetric and hermitian fields, respectively. Dropping the "site" index on the cluster fermions, the replicated disorder averaged action takes the form $\sum_{ab} S_0[\psi] + NS_1[c] + NS_2(\rho, \sigma, Q, P)$ with

$$S_0[\psi] = \int d\tau d\tau' d^d x \, \bar{\psi}_{ax\tau} \left(\delta_{ab}\partial_\tau - \delta_{ab}\xi(\partial_x) - \frac{g}{2}\delta^d(x - r_{imp})(\rho_{ab} + \mathbf{i}\sigma_{ab})\right) \psi_{bx\tau'},$$

$$S_1[c] = \int d\tau d\tau' \, \bar{c}_{a\tau} \left(\delta_{ab}\partial_\tau + \frac{g}{2}(\rho_{ab} - \mathbf{i}\sigma_{ab}) - Q_{ab}P_{ba}\right) c_{b\tau'},$$

$$S_2(\rho, \sigma, Q, P) = \frac{1}{2} \int d\tau d\tau' \left(\rho_{ab}^2 + \sigma_{ab}^2 + \frac{1}{2J^2} Q_{ab}^2 + Q_{ab} |P_{ab}|^2\right).$$

10

The saddle point equations for $Q, P, \rho,$ and σ resulting from this effective action give us the standard SYK saddle point results

$$P_{ab} = \langle \bar{c}_{a\tau} c_{b\tau'} \rangle, \quad Q_{ab} = J^2 |P_{ab}|^2$$

supplemented by two additional relations for the fields $\rho \pm \mathbf{i}\sigma$.

$$\rho + \mathbf{i}\sigma = -g \langle \bar{c}_{a\tau} c_{b\tau'} \rangle, \quad \rho - \mathbf{i}\sigma = \frac{g}{N} \langle \bar{\psi}_{a\tau, x=0} \psi_{b\tau, x=0} \rangle.$$

Upon integrating out ψ and c degrees of freedom, and assuming no replica symmetry breaking (and setting the position of the cluster at the origin $r_{imp} = 0$) one finds the effective action ($e^{-NS_{eff}} \equiv \int [DcD\psi] e^{-S}$),

$$S_{eff} = S_2(\rho, \sigma, Q, P) - \ln \det \left(\partial_\tau - QP + \frac{g}{2}(\rho - \mathbf{i}\sigma) \right) - \frac{1}{N} \ln \det \left(\partial_\tau - \xi(\partial_x) - \frac{g}{2}\delta^d(x)(\rho + \mathbf{i}\sigma) \right).$$

We can identify

$$\Sigma_{SYK} = J^2 \mathcal{G}|\mathcal{G}|^2 + \frac{g^2}{N} G_\psi(x, x), \quad \Sigma_\psi = g^2 \mathcal{G}_{syk}$$

which reproduces the previous result. In fact the replica analysis goes a step beyond the analysis of the previous section: it sums the series of corrections to the SYK propagator in powers of g^2/N, of which we only explicitly analyzed the first term. The $\delta(x)$ in these equations appears because we studied a single impurity, and yields a momentum-independent self energy upon Fourier transforming.

3 Towards finite N

3.1 Renormalization group analysis of impurity problem

Consider a single SYK cluster coupled to the itinerant mode. There is quite a bit of physics in this impurity problem, and it will be an extremely useful starting point. As we noted in §2.3, the large-N analysis is basically identical.

Weak coupling. First consider the regime where $g \ll t, J$. In this case, the correlation length of ψ is large compared to the lattice spacing, and we can treat the itinerant fermions in the continuum. Following the literature on the Kondo problem [45], only the s-wave mode of the Fermi surface $\psi_0(k) \sim k \int d\hat{\Omega} \psi(\Omega k)$ couples. Linearizing the s wave mode near the fermi surface with a bandwidth cutoff Λ the Hamiltonian for the left/right moving fields $\psi_{L/R} = \int_{-\Lambda}^{\Lambda} dk \, e^{\pm ikr} \psi_0(k + k_f)$ is [45]

$$H_{FS} = \frac{v_F}{2\pi} \int_0^\infty dr \left(\psi_L^\dagger \partial_r \psi_L - \psi_R^\dagger \partial_r \psi_R \right)$$

11

This implies that the free fields under consideration have mass dimension $[\psi_{L/R}] = \frac{1}{2}$. The scaling dimension of the SYK fields was determined in the low energy analysis in the previous section and found to be 1/4 for the fermion field and 3/4 for the bath field. The perturbation we are considering are of the forms

$$\Delta H = g\psi_L^\dagger(0)\chi, \qquad \Delta \tilde{H} = \tilde{g}\psi_L^\dagger(0)\tilde{\chi}.$$

The scaling dimension of the coupling constant g determines whether the hybridization becomes more or less important at low energies. Demanding that the action is dimensionless, the coupling to the bath field has mass dimension $-[\int dt\ \psi^\dagger\tilde{\chi}] = -\left(-1 + \frac{1}{2} + \frac{3}{4}\right) = -\frac{1}{4}$ and is therefore irrelevant. The coupling to the fundamental field χ has dimension $-[\int dt\ \psi^\dagger\chi] = -\left(-1 + \frac{1}{2} + \frac{1}{4}\right) = +\frac{1}{4}$, and is therefore relevant. Here again we depart from the holographic construction, where $\mathcal{G} \sim \omega^{2\nu}$ with positive ν – according to the above analysis the construction studied here, only $\mathcal{G}$ with negative ν can dominate the infrared physics.

Strong coupling. Now consider the regime where $g \gg t, J$. This is a highly-underscreened Anderson model. At each site, the itinerant fermion $\psi(x)$ is coupled to a particular linear combination $\frac{1}{N}\sum_i g_i\chi_i(x) \equiv \tilde{\chi}_N(x)$ of the SYK fermions at site x. Take linear combinations of the χ_i to orthogonalize the first $N-1$ with $\tilde{\chi}_N$. Then in the limit where $|g \gg J|$ (where g is the average of the g_i), we can simply neglect the four-fermion interactions involving $\tilde{c}_N$ and the result of the hybridization is simply to pair up $\psi(x)$ and $\tilde{\chi}_N(x)$ at each site, leaving behind at low energy only $N-1$ decoupled SYK clusters. This can be called a reverse Kondo phase: whereas the Kondo effect describes the absorption of an impurity into the Fermi sea of conduction electrons, here the situation is reversed: the impurities absorb the conduction electrons!
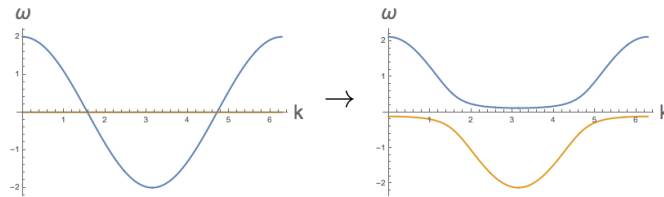

Figure 6: When $g \gg J$, we can neglect the SYK interactions, and our problem becomes quadratic. Hybridizing a localized fermion (flat band) with an itinerant fermion produces this bandstructure.

3.2   Possibilities for the phase diagram

Considerations of the topology of coupling space constrain the possibilities for the low-energy behavior of our system. Given that g is a relevant perturbation of the decoupled

fixed point with $g = 0$, and given that at large g, it produces a mass gap, the possible RG flow diagrams are as follows:
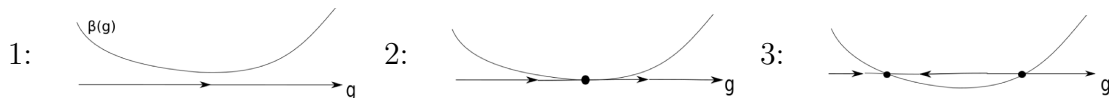

Figure 7: Possible behaviors of the beta function for g, given the known asymptotics. Arrows point toward the infrared.

The middle case (2) is nongeneric[4]. Therefore, if we find a fixed point, it is stable. In the following section, we will study the half-chain entanglement entropy. The above scenarios for the beta function would imply the following rough consequences for this quantity, respectively:
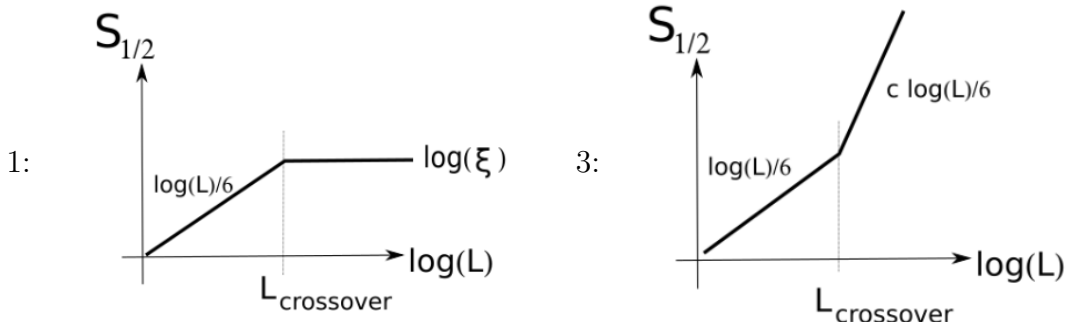

Figure 8: Behavior of the half-chain entanglement entropy in scenarios 1 and 3 of Fig. 8.

The respective scenarios *would* imply these behaviors of the half-chain entropy *if* the system were translation invariant. Although there are examples of highly-disordered fixed points which exhibit logarithmic area-law violation [47, 48], it is not clear whether this is inevitable.

We note that the behavior in scenario 3 does not violate RG monotonicity [49] of the 'central charge', because the UV fixed point is tensored with decoupled, localized clusters and is not a field theory. More generally, in a system without Lorentz symmetry, $\left(\frac{d}{d\log L}\right)^2 S_{\frac{1}{2}}$ may be positive. There are indeed known examples of disordered [50] and otherwise non-relativistic systems [51] where the 'central charge' (coefficient of

---

[4]A well-known example where the beta function has a double zero is in the BCS phase diagram, where $\beta(V) \propto V^2 + \dots$. Here the double zero occurs at the free theory, and is therefore protected by dimensional analysis.

13

$\log L$) increases towards the infrared. Note further that the condition we are violating, $\left(\frac{d}{d \log L}\right)^2 S_{\frac{1}{2}} < 0$, is a stronger condition than $\frac{d^2}{dL^2} S_{\frac{1}{2}} < 0$. In any case, the quantity $S_{\frac{1}{2}}(L)$ does not obey a known convexity theorem analogous to that of [52], which applies instead to the entanglement entropy as a function of subsystem of size ℓ of a *fixed* total system[5].

4   Coupling a Fermi surface to SYK$_{2.0001}$ clusters

In the limit $q \to 2$, the coupling $\int \psi \chi^\dagger$ becomes marginal. Therefore, in this limit, there is a hope that the NFL fixed point we're after can be accessed perturbatively in g. Indeed, as we sketch here, this seems to be the case.

Consider the replicated and disorder-averaged euclidean partition function[6] at $T = 0$

$$Z^n = \int [d\psi d\chi] e^{-S_0 - g^2 a^{2-2\Delta(q)} \int d\tau \int d\tau' \sum_{x,i} \psi_x(\tau) \chi_{xi}(\tau)^\dagger \chi_{xi}(\tau') \psi_x(\tau')^\dagger}.$$

Replica indices accompany the time labels and are suppressed. Here S_0 is the action for the fixed point described by a Fermi surface

$$\left\langle \psi^\dagger(\omega, k) \psi(\omega, k) \right\rangle_0 = \frac{1}{\mathbf{i}\omega - v_F |k - k_F|}$$

times decoupled SYK$_q$ clusters at each site *in their conformal limit,*

$$\left\langle \chi^\dagger(\tau) \chi(0) \right\rangle_0 = C(J) \mathrm{sign}(\tau) |\tau|^{-2/q}.$$

Here $C(J) = C J^{-2/q}$ with $C > 0$ [22, 53]. The factor of $a^{2-2\Delta(q)}$ (where $2 - 2\Delta(q) = \frac{q-2}{q}$ is the scaling dimension of $\chi\psi^\dagger$)) has been pulled out of g to make g dimensionless.

We implement the RG as in [54], by expanding

$$Z^n = Z^n_\star \left(1 - g^2 \left\langle \int d\tau \int d\tau' \psi(\tau) \chi(\tau)^\dagger \chi(\tau') \psi(\tau')^\dagger \right\rangle_0 \right.$$
$$\left. + g^4 \left\langle \int d\tau \int d\tau' \psi(\tau) \chi(\tau)^\dagger \chi(\tau') \psi(\tau')^\dagger \int d\tau'' \int d\tau''' \psi(\tau'') \chi(\tau'')^\dagger \chi(\tau''') \psi(\tau''')^\dagger \right\rangle_0 + \cdots \right).$$

$$(4.1)$$

---

[5]Thanks to Tarun Grover for helpful discussions of these constraints on the behavior of $S(\ell, L)$.

[6]In many disordered systems, one must consider the RG evolution of the probability distribution for the disorder. The renormalization group strategy pursued here, of studying the flow of the disorder-averaged action, *assumes* that the Gaussian disorder-distribution for g_{ix} is self-similar under an RG transformation – we are allowing only its variance g to evolve.

We wish to let $g = g(a)$ run with the UV cutoff a in such a way as to cancel the dependence of Z on a, perturbatively in g. The cutoff dependence appears explicitly in the perturbation term and implicitly in the need to regulate collisions of the integrations $|\tau - \tau''| > a$.

The contractions in the $\mathcal{O}(g^2)$ term produce corrections to the renormalized action of the form

$$\delta S = g^2 \int d\tau \left(\psi^\dagger(\tau)\psi(\tau)A + \chi^\dagger(\tau)\chi(\tau)B \right)$$

where

$$
\begin{aligned}
B &= \int_a d\tau \left\langle \psi^\dagger(\tau, x)\psi(0, x) \right\rangle_0 = \int_a d\tau \int đ\omega e^{-i\omega\tau} \int \frac{đ^d p}{i\omega - v_F|p - k_F|} \\
&= \int_a d\tau \int đ^d p\, e^{-v_F p_\perp \tau} \\
&\simeq \frac{1}{2} \int_{-\beta}^{\beta} d\tau \underbrace{\frac{\Omega_{d-1}}{(2\pi)^d}}_{\equiv K_d} k_F^{d-1} \underbrace{\int dp_\perp e^{-i v_F p_\perp \tau}}_{= \frac{1}{v_F \tau}} = -\frac{K_d k_F^{d-1}}{v_F} \left(\int_{-\beta}^a + \int_a^\beta \right) \frac{d\tau}{\tau} = 0 \quad (4.2)
\end{aligned}
$$

and

$$A = \int_a d\tau \left\langle \chi^\dagger(\tau)\chi(0) \right\rangle_0 = C(J) \int_a d\tau \operatorname{sign}(\tau)|\tau|^{-2/q} = 0.$$

In (4.2), β was introduced as an IR regulator[7]. A, were it nonzero, would be an innocuous correction to the ψ chemical potential. Away from half-filled clusters, where $|\mathcal{G}(\tau)| \neq |\mathcal{G}(-\tau)|$, we find $A \sim a^{1-2/q}$. Similarly, B would be a correction to the chemical potential for χ. In [22, 53], such a chemical potential is included in the analysis; the phase of $\mathcal{G}$ depends on it, but it is otherwise innocuous as well.

The interesting term for us is the (connected) contraction of the g^4 term which renormalizes g^2. This is

$$
\begin{aligned}
\delta g^2 &= -\frac{1}{2} \quad \text{} \\
&= (-1)^2 \frac{1}{2} \int_a d\tau \left\langle \chi^\dagger(\tau)\chi(0) \right\rangle_0 \left\langle \psi^\dagger(\tau, x)\psi(0, x) \right\rangle_0 + h.c. \\
&\simeq \frac{1}{2} C(J) \frac{K_d k_F^{d-1}}{v_F} \int_a d\tau \tau^{-2/q} \tau^{-1} \simeq \frac{1}{2} C(J) \frac{K_d k_F^{d-1}}{v_F} a^{-2/q} . \quad (4.3)
\end{aligned}
$$

The minus sign in the first line is from the relative sign between the $\mathcal{O}(g^4)$ term and the $\mathcal{O}(g^2)$ term in (4.1). The minus sign in the second line is from the fermion loop –

---

[7] Note that since zero is a bosonic matsubara frequency, it is important that we integrate from $-\beta$ to β (and divide by two), rather than just a to β. The latter would give $B \overset{?}{\sim} \log aT$. Thanks to Aavishkar Patel for patient explanations of this point.

we are contracting non-adjacent fermion operators. Crucially, $C(J)$ is *positive* for all values of the parameter θ (which is determined by the filling).

Therefore,

$$\beta_{g^2} \equiv \frac{d}{d\log a}g^2 = (2 - 2\Delta(q))g^2 + \frac{1}{2}C(J)\frac{K_d k_F^{d-1}}{v_F}\left(-\frac{2}{q}\right)g^4 + \mathcal{O}(g^6).$$

Here

$$2 - 2\Delta(q) = \frac{q-2}{q} = 1 - \frac{2}{2+\epsilon} = \epsilon + \mathcal{O}(\epsilon^2), \quad -\frac{2}{q} = -\frac{2}{2+\epsilon} = -1 + \epsilon + \mathcal{O}(\epsilon^2).$$

Besides the trivial fixed point at $g = 0$, this indicates a fixed point $0 = \beta_{g^2}(g = g_\star)$ at

$$g_\star^2 = \frac{2v_F}{C(J)K_d k_F^{d-1}}\epsilon + \mathcal{O}(\epsilon^2),$$

which is indeed at weak coupling, parametrically in ϵ. We note that it is also parametrically small in the area of the Fermi surface, k_F^{d-1}, suggesting that perhaps the physics at $q = 4$ can be captured by this analysis. The fixed point depends on J like $g_\star^2 \sim C(J)^{-1} \sim J^{2/q}$.

5 Numerical analysis

We have attempted to perform some quantitative studies of the model considered in this paper, in the special case of a one-dimensional chain. We use the standard technique for numerical studies of one dimensional systems, the density matrix renormalization group (DMRG) [55]. Specifically, we use a single site matrix product state sweeping algorithm [56]. There are several factors which make it difficult to study this system numerically.

The unusually large size of the local Hilbert space at each site (which is $2^{N_{syk}+1}$, as opposed to 2 for a spin 1/2 chain or 4 for spinful fermions) means that the computational resources required at a given bond dimension are significantly larger than what is needed for studying spin chains. Furthermore, as is the case in most studies of systems with quenched disorder, we are interested in correlation functions averaged over many disorder realizations. Therefore, at each set of coupling constants, we must perform enough trials to achieve convergence. In some cases the number of trials required is relatively small (~ 50) and in other cases it is larger (~ 500).

We use two different methods for our DMRG study. One is a completely standard MPS based DMRG sweeping algorithm in which we take $N_{syk} = 6$ on each site. This

number is not very large, but is perhaps comparable to the numbers one might hope for in material realizations of such a model.

The other method, which we'll refer to as the truncation method, begins with $N_{syk} = 12$ on each site. The size of the local Hilbert space here is too large to work with in our DMRG algorithm, so we form an isometry which projects the Hamiltonian into the subspace spanned by the $128 = 64 * 2$ lowest energy eigenstates. That is, we exactly diagonalize $\mathbf{H}_{syk}$ with 12 modes in the presence of one extra fermionic mode which the Hamiltonian doesn't act on. So we truncate a Hilbert space of the form $2^{12} \otimes 2 \rightarrow 64_{syk} \otimes 2$. The entire Hamiltonian, as well as the hybridization and hopping terms, are projected into this truncated space.

The idea behind the truncation approach is that the properties of interest (in particular, the singular self-energy) arise due to the special low energy physics of the SYK cluster. The expressions given for the Green's functions of the large N theory considered in section 2.2 were all valid at low energies and at momenta near the Fermi surface. The relevant energy scales to compare are the hybridization coupling g and the bandwidth D of the states that are retained. This is found to be $D \sim 0.26J$ at $N_{syk} = 12$.

To help map out the phase diagram, one of the most convenient and easily accessible quantities we can measure is the entanglement entropy of subregions of the chain (EE). In particular, (a review is [57]) a one dimensional conformal field theory (CFT) in the thermodynamic limit has an entanglement entropy which grows with the size L of the subregion as $\frac{c}{3} \log L$, where c is the central charge of the CFT[8]. Similarly, for a CFT on a space of length L, the half-chain entanglement entropy scales with the system size as $\frac{c}{6} \log L$. Thus, measuring the growth of the half-chain entanglement entropy with the system size allows us to access some universal information about the phase and its low-energy excitations, from just the groundstate wavefunction. We note that the emergence of Lorentz symmetry, much less conformal symmetry, is unlikely in our disordered system, so the measured behavior of the entanglement entropy is a proxy for the number of low-energy degrees of freedom.

Considering fixed J, we know the behaviour of the half-chain EE at both small g and very large g. At zero g, the SYK clusters are decoupled from the free fermion chain. The latter is responsible for all of the spatial entanglement, and has $c = 1$ for spinless fermions. That is what we observe from the slope of the half chain EE. At large g, the hybridization term dominates and we expect the itinerant fermions to bind into a local singlet. This phase has a finite correlation length which becomes very small at large g. Hence the EE satisfies an area law and $c = 0$. We observe this behaviour

---

[8]For simplicity, we assume a non-chiral spectrum.

in our simulations.

As g increases from zero, there are two possibilities, as we discussed in §3. Although finite size effects are hard to overcome in our particular model, measuring the slope of the half chain EE at different values of g provides some evidence for either scenario 1 or 3 above.
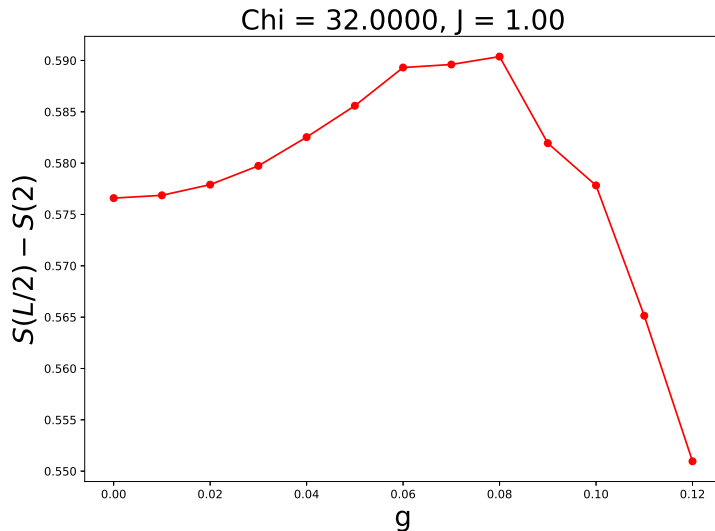

Figure 9: The half-chain entanglement $S(L/2) - S(2)$ at fixed $L = 52$, as a function of g, averaged over up to 600 samples.

Half-chain entropies. In Fig. 9 we plot $S(L/2) - S(2)$ at fixed L for various g, and observe smooth growth to a maximum value, suggestive of scenario 3 with an intermediate-coupling fixed point. $S(2)$ is subtracted to remove a g-dependent constant shift. Beyond the maximum, all the entanglement is destroyed; this is the reverse Kondo phase.

The right panel of Fig. 10 illustrates the fact that the coupling to bath field $\tilde{g}\psi\tilde{\chi}$ is irrelevant – it is identical to the free fermion answer for all $\tilde{g}$.

The left panel of Fig. 10 shows the half-chain entanglement entropy as a function of $\log(L)$ for $J = 2, t = 1$, and various values of g, computed using the truncation scheme. We expect these choices of J and g are in the regime of validity of the truncation especially for the smaller values of $g \lesssim D/10$. For comparison, the results obtained using the standard DMRG are shown in Appendix B.

There is a regime at small g where the entanglement grows faster with L than the free-fermion answer at small system sizes At larger L, the curve levels off to approximately the same slope as the free-fermion curve. One possibility is that this is due
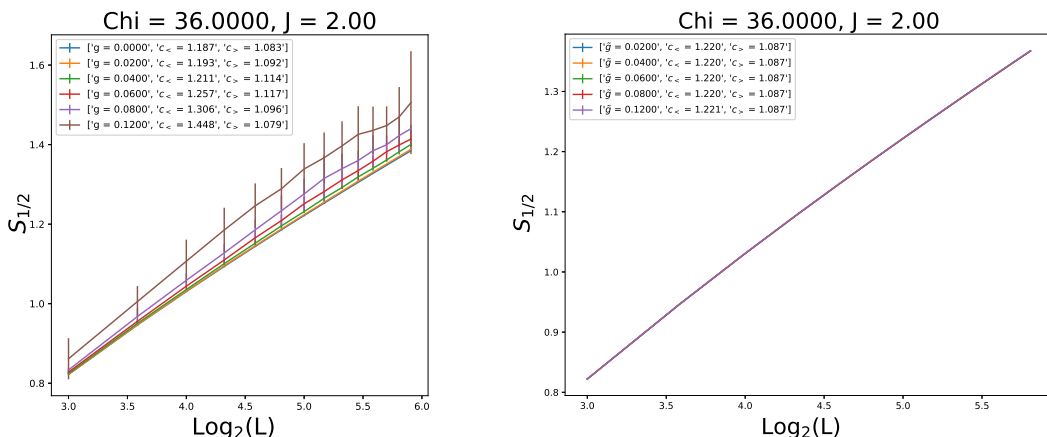
Figure 10: Left: half-chain entanglement entropy versus log of system size for $J = 2, t = 1$, and various values of g, the coupling to the fermion field, computed in the truncated scheme. $c_<$ and $c_>$ are six times the slope calculated at $\log_2 L < 5$ and $\log_2 L \geq 5$ respectively. Right: half-chain entanglement entropy versus log of system size, for various values of $\tilde{g}$, the coupling to bath field. In the latter case, the curves all lie on top of the free fermion curve. The inset gives fits to the slope (times 6).

to some extra finite-range correlation between the cluster degrees of freedom on top of the extended contribution from the itinerant degree of freedom, and that the true area law violating term has the same coefficient as a decoupled spinless fermion.

Another possiblity is that the apparent rejoining with the free fermion value is related to a previously-observed difficulty in the use of DMRG algorithms for disordered critical systems [58]. If we parametrize the EE as

$$S_{1/2}(L) = \frac{1}{6} \log_2 L + \frac{\delta c_{dis}}{6} g(L) + const,$$

where $g(x) = \log_2(x)$ at $x < l_{crossover} \sim 2^5$ and saturates to a constant at $x \gtrsim l_{crossover}$, this reproduces our observed results. A more conservative explanation is that $c \sim 1$ throughout the extended phase.

In addition to the scaling of the EE with the system size, we can also look at the dependence on the size of the bipartition at fixed system size. Fitting our data to known expressions for the finite size entanglement in critical systems [59, 60, 61] provides another method to extract the 'central charge'. The quality of the fit is also a useful diagnostic of whether the system is approximately critical or has a finite correlation length. Our results are shown in Figure 11; at small g we observe a small rise in the entanglement but cannot draw a strong conclusion. At larger values of g we observe the onset of a finite correlation length.
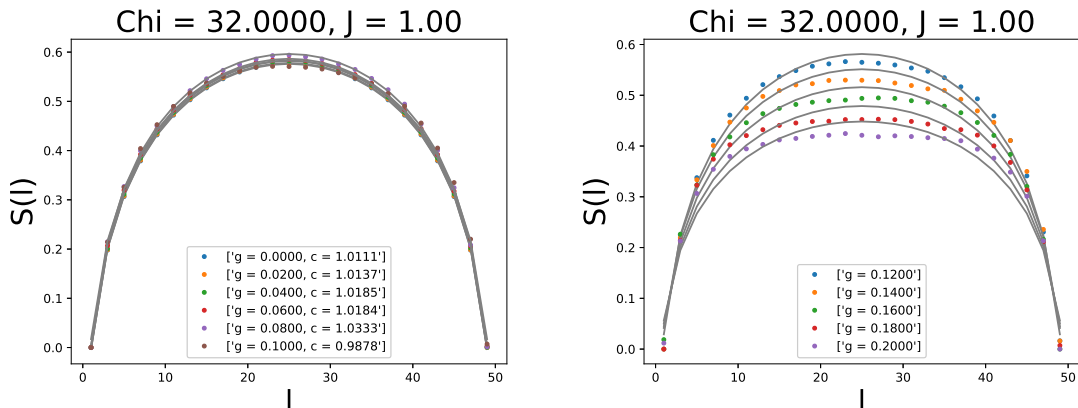
Figure 11: The finite size entanglement as a function of the position of the entanglement cut at a fixed system size $L = 52$. We plot only the even sites in order to remove even-odd oscillations. At small values of g, the data is well fit by the expression $S(x) = \frac{c}{6} \log_2 \left(\frac{2L}{\pi} \sin(\pi x/L) \right) + a$. At larger values of g the fit fails. Data are averaged over $200 - 400$ disorder realizations.

Correlation functions. Fig. 12 shows the fermion equal-time correlation functions in the DMRG approximation to the groundstate. The absolute value is averaged over 50 instances.

The result fits well to

$$\left| \left\langle \psi_x^\dagger \psi_{L/2} \right\rangle \right| \sim \frac{|\sin 2k_F(x - L/2)|}{|x - L/2|^\alpha} \tag{5.1}$$

with $\alpha < 1$. The free fermion answer is of the form (5.1) with $\alpha = 1$. For $g > 0$, the exponent is larger than the free fermion value. It would be interesting to try to reproduce this change in the exponent using the $q - 2$ expansion. The right column of Fig. 12 shows that at the same values of g, the so-called localized fermions χ are indeed still localized. The bottom row of Fig. 12 shows that at large g, everybody is localized – this is the reverse Kondo phase.

Lesion studies. To what extent is the use of the SYK model as the cluster Hamiltonian crucial? We can attempt to address this question by perturbing the cluster Hamiltonian by (relevant) quadratic terms. In the case of purely quadratic clusters, the entire Hamiltonian is quadratic, and we can study larger system sizes, calculating the entropy by the Peschel formula [62]. The result is shown in Fig. 13.

Another reason to study the case of quadratic clusters is to identify the length scale at which localization sets in. In one dimension, to which our numerical work is sadly limited, localization is likely the inevitable long-distance fate. We see in Fig. 13 that at $g \lesssim 0.3$ localization sets in at system sizes which are too large for us to accurately study using DMRG. Therefore we cannot rule out the possibility that the quartic model
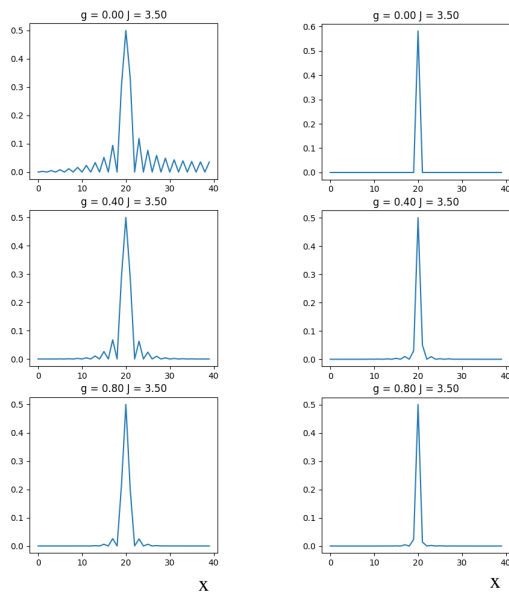
Figure 12: Left: The absolute value of correlation functions of the itinerant ψ fermions between the middle site and the site x, for various g. Right: The absolute value of correlation functions of the localized χ fermions between the middle site and the site x, for various g.

would show a finite correlation length as well at larger system sizes. However, whereas localization is guaranteed for the disordered quadratic system in one dimension [63], it is possible that the interacting system remains extended.

6 Conclusions

In this paper we have studied what happens when we couple a Fermi surface to a lattice of locally critical clusters. We have provided evidence from various approaches for the existence of a novel strange metal fixed point at intermediate values of the root-mean-square hybridization coupling g. This fixed point is stable to perturbations of g. Intra-cluster quadratic terms are likely to be relevant. We note that the proposed new strange metal fixed point is not Lorentz invariant.

A comment about the role of large N is in order. The power-law in the SYK fermion Green's function is a crucial ingredient in the construction. Such critical behavior in a (0+1)-dimensional system requires a large number of degrees of freedom: if one takes $\omega \to 0$ before $N \to \infty$, the low-lying level spacing of the clusters will be discrete. The effects of this phenomenon are visible in the top left of Fig. 3: if the level spacing of the SYK clusters is large compared to t and g, the hybridization coupling has no effect.
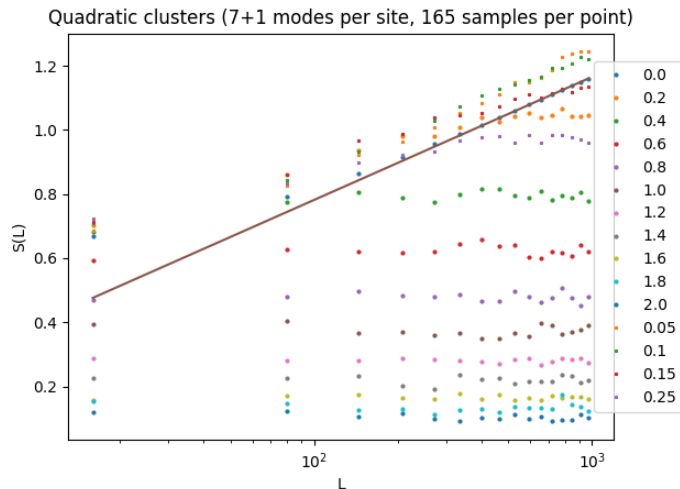
Figure 13: Half-chain entropy as a function of chain length for a free-fermion chain (uniform hopping $t = 1$) hybridized with local *quadratic* clusters, with random quadratic intra-cluster interactions of mean 1. Different curves are different values of the root-mean-square hybridization coupling g, which varies from 0 to 2.0. The solid line is the asymptotic behavior in the clean limit, $S(L) = \frac{1}{6} \log(L) + a$.

At leading order in large-N, the power-law in the cluster-fermion Green's function is directly carried over into the itinerant fermion self-energy, as in the holographic calculation. In contrast, at finite N, only power-laws corresponding to relevant perturbations (in the sense of §3) affect the low-energy behavior of the itinerant fermions. The bath field $\tilde{\chi}$, for example, is irrelevant for all q. This restricts the resulting states to have self-energy exponent $2\nu < 0$.

We should emphasize that the stability of the putative strange metal fixed point is predicated on not adding other (quadratic) operators to the SYK cluster hamiltonian. (Such relevant deformations are also visible in the semi-holographic description [9].) So inevitably, the physics we have discussed should only be realized at intermediate temperatures.

The title of the paper merits a comment. Its maximal chaos is a signature property of the SYK model, and this justifies our use of the term 'local quantum chaos' for the behavior of the clusters. This maximal quantum chaos is a property of the states in the middle of the spectrum. In contrast, the essential ingredient for our construction is the power-law behavior in frequency of the groundstate and low-temperature Green's functions. The absence of quasiparticles certainly requires breaking of integrability, as borne out by the data show in Fig. 13. But whether there is indeed an intimate connection between these different facets of the physics of SYK is an interesting open question.

We conclude with a suggestion for a direction for progress towards corroborating the existence of this fixed point and studying its properties. The matrix product ansatz used in the DMRG study of §5 does not take advantage of all of the structure of the problem. In particular, the fact that the clusters do not couple directly to each other represents a kind of 'entanglement bottleneck' – any long-ranged entanglement along the chain necessarily passes through the itinerant fermion sites. To take advantage of this, it would be useful to construct a variational tensor product state with the structure of our interaction graph shown in Fig. 1. It would also be interesting to try to apply an adaptation of the dMera of [58] to answer the question regarding the scaling of the EE in our disordered system.

A $\quad 1/N$ corrections to the cluster-fermion propagator

As promised in §2, here we analyze the $1/N$ correction to the propagator of the localized fermions. Starting from the conformal SYK propagator as $\mathcal{G}_0$, and denoting convolution over the intermediate variable by $*$, we have

$$\mathcal{G}(\omega, x - y) - \mathcal{G}_0(\omega)\delta_{xy} = \frac{g^2}{N}\mathcal{G}_0(\omega)^2 G_{xy}^0\delta_{xy} + \frac{g^4}{N}\mathcal{G}_0(\omega)^3\delta_{xy}G_{xz}^0 * G_{zy}^0 + \dots$$

Fourier transforming and using results from §2, we find

$$\delta\mathcal{G}(k\omega) = N^{-1}\left(g^2\mathcal{G}_0^2(\omega)\int \text{đ}k\, G^0(k\omega) + g^4\mathcal{G}_0^3\int \text{đ}k\, G^0(k\omega)^2 + \dots\right)$$

$$= \frac{g^2}{N}\int \text{đ}k\mathcal{G}_0^2\frac{1}{G_0(k)^{-1} - g^2\mathcal{G}_0} = \frac{g^2}{N}\mathcal{G}_0^2\int \text{đ}kG(k).$$

$$= \frac{g^2}{N}\mathcal{G}_0^2(\omega)\int \text{đ}^dk\ \frac{1}{\mathbf{i}\omega - \xi(k) + \mathbf{i}g^2(\pi/J^2)^{1/4}|\omega|^{-1/2}\text{sgn}\ \omega}$$

Analysis of the integral. Thus the $1/N$ correction to the localized fermion propagator is proportional to

$$D(\omega) \equiv \int \text{đ}^dkG(k, \omega) = G(\omega; xx), \tag{A.1}$$

the local density of states of the itinerant fermions, the quantity which determines the dI/dV curve measured by scanning-tunneling microscopy.

Some difficulty arises from the UV-sensitivity of this integral: the answer is not a property of only the physics at the Fermi surface, but depends also on short-distance details. Here we will show that, given the form of the SYK propagator $\mathcal{G}_0(\omega)$, the resulting $D(\omega)$ *vanishes* at small frequency, independent of those short-distance details. Therefore, this $1/N$ correction does not modify the leading low-frequency scaling behavior of $\mathcal{G}$, even at frequencies very small compared to N.

Let us parametrize G as follows:

$$G(k, \omega) = \frac{1}{\omega - \xi(k) - \Sigma(\omega)}. \tag{A.2}$$

(Note that we assume k-independent self-energy.) To learn something about integrals of the form (A.1), consider free fermions with bandstructure $\xi(k)$, in which case we have the Schwinger-Dyson equation

$$(-\mathbf{i}\partial_t + \xi(\mathbf{i}\partial_x)) G_{x,0}(t) = \delta^d(x)\delta(t)$$

and hence by Fourier transform

$$G(k, \omega) = \int dt d^d x e^{-\mathbf{i}(kx - \omega t)} G_{x,0}(t),$$

(A.2) obtains with $\Sigma(\omega) = 0$. On the other hand, we also have

$$G_{x,0}(t) \equiv \langle \mathrm{gs}| c_x^\dagger(t) c_0(0) |\mathrm{gs}\rangle = \int \bar{d}^d k \int \bar{d}^d q \, \langle \mathrm{gs}| e^{-\mathbf{i}\omega_k t + \mathbf{i}kx} c_k^\dagger c_q |gs\rangle = \int_{q \in FS} \bar{d}^d q e^{-\mathbf{i}\omega_q t + \mathbf{i}qx}.$$

Therefore

$$D(\omega) = \int \bar{d}^d k \int dt d^d x e^{-\mathbf{i}(kx - \omega t)} \frac{1}{V} \sum_{q \in FS} e^{-\mathbf{i}\omega_q t + \mathbf{i}qx} \tag{A.3}$$

$$= \int dt e^{\mathbf{i}\omega t} \int_{q \in FS} \bar{d}^d q e^{-\mathbf{i}\omega_q t} \tag{A.4}$$

$$= \int_{q \in FS} \bar{d}^d q \delta(\omega - \omega_q) \tag{A.5}$$

$$= \int_{q \in FS} \bar{d}^d q \frac{\delta(q - q(\omega))}{\partial_q \omega} = \theta(\mu - \omega)\rho(\omega) \tag{A.6}$$

which is the density of filled levels. Notice that (A.6) correctly reproduces

$$\int d\omega D(\omega) = \int \bar{d}^d q G_q(t = 0) = \int \bar{d}^d q \, \langle gs| c_q^\dagger c_q |\mathrm{gs}\rangle = \int_{q \in FS} N_q = N$$

the total number of fermions.

For example, consider the case when the Fermi level is near the edge of a 1d band, so that $\rho(\omega) = \frac{1}{\sqrt{\omega - 2t}}\theta(2t - \omega)$. Let us reproduce this answer using (A.6) starting from the Green's function (A.2). Linearizing about the Fermi surface $k_\perp = k - k_F$,

$$\xi(k) = -\mu + v_F k_\perp + \mathcal{O}(k_\perp)^2 \tag{A.7}$$

would give

$$D(\omega) \overset{?}{=} \Omega_d k_F^{d-1} \int_{-\Lambda}^{\Lambda} dk_\perp \frac{1}{f(\omega) - v_F k_\perp} = \Omega_d k_F^{d-1} \log\left(\frac{f(\omega) - v_F \Lambda}{f(\omega) + v_F \Lambda}\right)$$

which depends on Λ at large Λ – this is the UV sensitivity we advertised above. The answer will be different if we include the next term in the expansion (A.7) about the Fermi surface:

$$\xi(k) = -\mu + v_F k_\perp + t k_\perp^2 + \dots$$

since then the integral $\sim \int^\Lambda \frac{dk_\perp}{k_\perp^2}$ would be finite as $\Lambda \to \infty$. For definiteness, focus on the 1d band edge example: that is, suppose $d = 1$ and μ is near the bottom of the band so $v_F = 0$. Then

$$D(\omega) = \int_{-\infty}^{\infty} đk \frac{1}{\omega - t k^2} = \frac{1}{\sqrt{\omega t}}$$

(the contour can be closed in either half-plane). The imaginary part is only nonzero for $\omega < 0$, and reproduces the divergence at the 1d band edge.

Armed with this intuition, we return to the case of interest, where at low frequency the singular self-energy dominates, and $f(\omega) \sim \omega^{-1/2}$. In that case (still in $d = 1$ for now),

$$D(\omega) = \int đk \frac{1}{C\omega^{-1/2} - \mu - \xi(k)} = \int đk \frac{\omega^{1/2}}{C - (\mu - \xi(k))\,\omega^{1/2}}.$$

Assume that ξ is a polynomial of degree D in k, $\xi = a_0 k^D + a_1 k^{D-1} + \cdots$; then letting $u \equiv \omega^{\frac{1}{2D}} k$, this integral at small ω is

$$D(\omega) = \omega^{\frac{1}{2} - \frac{1}{D}} \int đk \frac{1}{C - a_0 u^D + a_1 u^{D-1}\omega^{\frac{1}{2D}} + \cdots} \overset{\omega \to 0}{\sim} \omega^{\frac{1}{2} - \frac{1}{D}}$$

Alternatively, suppose the we are working in a lattice model, so that the momentum integral $\int đ^d k$ is over a finite Brillouin zone; in that case, $D(\omega) \overset{\omega \to 0}{\sim} \omega^{1/2}$. In either case, we find $D(\omega) \overset{\omega \to 0}{\to} 0$.

In general d, the same analysis gives

$$D(\omega) = \omega^{1/2} \int \frac{đ^d k}{\omega^{\frac{1}{2}} k^D + \dots} = \omega^{\frac{1}{2} - \frac{d}{2D}} K_d \int \frac{u^{d-1} du}{u^D + \cdots}$$

25

where $K_d = \frac{\Omega_{d-1}}{(2\pi)^d}$. The integral converges when $D > d$, in which case the power of omega is $\frac{1}{2} - \frac{d}{2D} > 0$, and the integral vanishes as $\omega \to 0$. Alternatively, we can appeal to the lattice regulator: compactness of the Brillouin zone guarantees that $D(\omega) \overset{\omega \to 0}{\to} \omega^{\frac{1}{2}} \int d^d k \frac{1}{C}$ is $\omega^{\frac{1}{2}}$ times a finite integral.
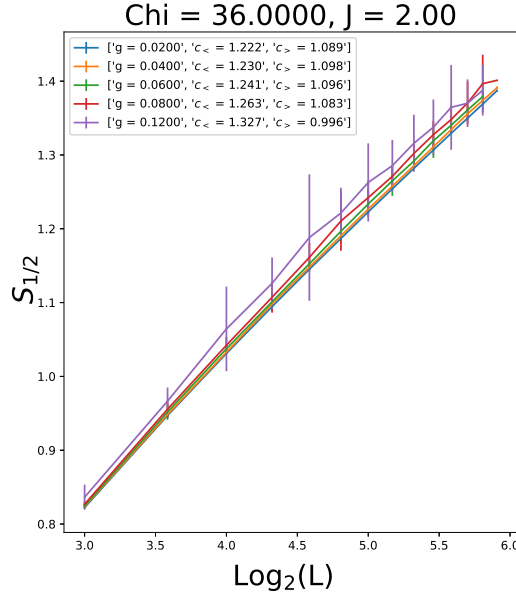
B   Other numerical results

Figure 14: $S_{1/2}$ vs Log(L) calculating using standard DMRG at small g.

The standard vMPS algorithm with only six cluster fermions is an especially poor representative of the large N model at very small g; if g is smaller than the finite size energy gap between the SYK ground state and the excited states then the hybridization interaction is essentially frozen out. The truncated version of the algorithm starting with a larger Hilbert space does a better job in representing the large N model.

A benchmark of the truncation method. The truncation method outlined above is an uncontrolled approximation for the sizes of local Hilbert spaces available to us. As a test of the method, in Fig. 15 we show the spectrum of an SYK impurity coupled to a single extra fermionic mode (one site of the chain). The bottom part of the truncated spectrum matches quite well with the correct spectrum. The top of the truncated spectrum is wrong: the level repulsion from the levels above is missing. We used this method in studying the growth of the half-chain entanglement entropy in
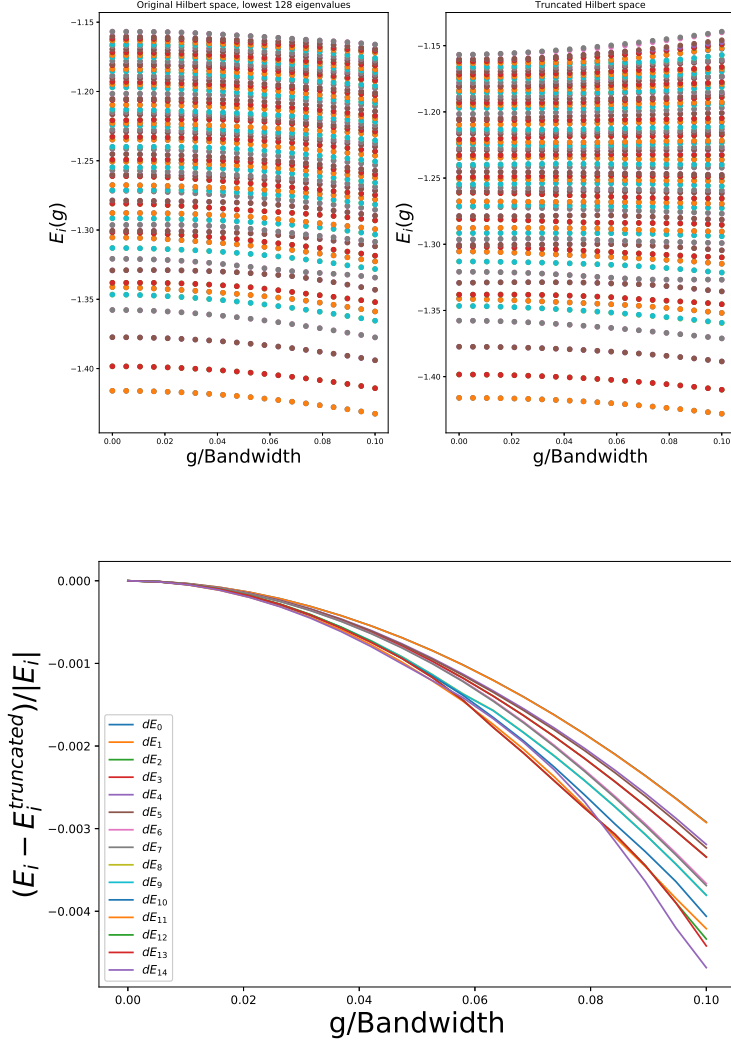
26

Figure 15: A check on the validity of the truncation method. Top Left: first 128 levels of an SYK cluster with $N_{syk} = 12$ hybridized with a single extra fermion mode. Top Right: the spectrum of the truncated SYK hamiltonian (truncated to 64 levels) coupled to an extra fermion mode. Bottom: Fractional error in the energy eigenvalues of the lowest fifteen states.

addition to the standard MPS algorithm.

Acknowledgements

using resources provided by the Open Science Grid [64, 65], which is supported by the National Science Foundation award 1148698, and the U.S. Department of Energy's Office of Science.

References

[1] S.-S. Lee, "Recent Developments in Non-Fermi Liquid Theory," *arXiv preprint* (2017) 1703.08172. 1

[2] S.-S. Lee, "A Non-Fermi Liquid from a Charged Black Hole: A Critical Fermi Ball," *Phys. Rev.* **D79** (2009) 086006, 0809.3402. 1

[3] H. Liu, J. McGreevy, and D. Vegh, "Non-Fermi liquids from holography," *Phys.Rev.* **D83** (2011) 065029, 0903.2477. 1

[4] M. Cubrovic, J. Zaanen, and K. Schalm, "String Theory, Quantum Phase Transitions and the Emergent Fermi-Liquid," *Science* **325** (2009) 439–444, 0904.1993. 1

[5] T. Faulkner, H. Liu, J. McGreevy, and D. Vegh, "Emergent quantum criticality, Fermi surfaces, and AdS(2)," *Phys.Rev.* **D83** (2011) 125002, 0907.2694. 1, 2, 4

[6] T. Faulkner, N. Iqbal, H. Liu, J. McGreevy, and D. Vegh, "Strange metal transport realized by gauge/gravity duality," *Science* **329** (2010) 1043–1047, 1003.1728. 1, 4

[7] J. McGreevy, "TASI lectures on quantum matter (with a view toward holographic duality)," 1606.08953. 1

[8] C. M. Varma, P. B. Littlewood, S. Schmitt-Rink, E. Abrahams, and A. E. Ruckenstein, "Phenomenology of the normal state of Cu-O high-temperature superconductors," *Phys. Rev. Lett.* **63** (Oct, 1989) 1996–1999. 2

[9] T. Faulkner and J. Polchinski, "Semi-Holographic Fermi Liquids," 1001.5049. 2, 22

[10] N. Iqbal, H. Liu, and M. Mezei, "Semi-local quantum liquids," *JHEP* **04** (2012) 086, 1105.4621. 2

[11] A. Allais, J. McGreevy, and S. J. Suh, "A quantum electron star," *Phys. Rev. Lett.* **108** (2012) 231602, 1202.5308. 2

[12] A. Allais and J. McGreevy, "How to construct a gravitating quantum electron star," *Phys. Rev.* **D88** (2013), no. 6 066006, 1306.6075. 2

[13] A. Georges, G. Kotliar, W. Krauth, and M. J. Rozenberg, "Dynamical mean-field theory of strongly correlated fermion systems and the limit of infinite dimensions," *Rev. Mod. Phys.* **68** (1996) 13–125. 2

[14] G. Kotliar, S. Y. Savrasov, K. Haule, V. S. Oudovenko, O. Parcollet, and C. A. Marianetti, "Electronic structure calculations with dynamical mean-field theory," *Rev. Mod. Phys.* **78** (2006) 865–951. 2

[15] K. Jensen, S. Kachru, A. Karch, J. Polchinski, and E. Silverstein, "Towards a holographic marginal Fermi liquid," *Phys. Rev.* **D84** (2011) 126002, 1105.1772. 2

[16] K. Jensen, "Chaos and hydrodynamics near AdS$_2$," 1605.06098. 2

[17] J. Maldacena, D. Stanford, and Z. Yang, "Conformal symmetry and its breaking in two dimensional Nearly Anti-de-Sitter space," 1606.01857. 2

[18] A. Almheiri and B. Kang, "Conformal Symmetry Breaking and Thermodynamics of Near-Extremal Black Holes," 1606.04108. 2

[19] S. Sachdev and J. Ye, "Gapless spin-fluid ground state in a random quantum Heisenberg magnet," *Physical Review Letters* **70** (May, 1993) 3339–3342, cond-mat/9212030. 3

[20] A. Georges, O. Parcollet, and S. Sachdev, "Mean Field Theory of a Quantum Heisenberg Spin Glass," *Physical Review Letters* **85** (July, 2000) 840–843, cond-mat/9909239. 3

[21] A. Kitaev, "A simple model of quantum holography," *unpublished* (2015) http://online.kitp.ucsb.edu/online/entangled15/. 3

[22] S. Sachdev, "Bekenstein-Hawking Entropy and Strange Metals," *Phys. Rev.* **X5** (2015), no. 4 041025, 1506.05111. 3, 5, 6, 10, 14, 15

[23] S. Sachdev, "Strange metals and the AdS/CFT correspondence," *Journal of Statistical Mechanics: Theory and Experiment* **11** (Nov., 2010) 22, 1010.0682. 3, 4

[24] S. Sachdev, "Holographic metals and the fractionalized Fermi liquid," *Phys.Rev.Lett.* **105** (2010) 151602, 1006.3794. 3, 4

[25] E. Miranda, V. Dobrosavljevic, and G. Kotliar, "Kondo disorder: a possible route towards non-Fermi-liquid behaviour," *Journal of Physics: Condensed Matter* **8** (1996), no. 48 9871. 4

[26] Y. Gu, X.-L. Qi, and D. Stanford, "Local criticality, diffusion and chaos in generalized Sachdev-Ye-Kitaev models," *Journal of High Energy Physics* **2017** (2017), no. 5 125. 4

[27] S. Banerjee and E. Altman, "Solvable model for a dynamical quantum phase transition from fast to slow scrambling," *Physical Review B* **95** (2017), no. 13 134302. 4

[28] A. Haldar and V. B. Shenoy, "Strange Half Metals and Mott Insulators in SYK Models," *ArXiv e-prints* (Mar., 2017) 1703.05111. 4

[29] X. Chen, R. Fan, Y. Chen, H. Zhai, and P. Zhang, "Competition between Chaotic and Non-Chaotic Phases in a Quadratically Coupled Sachdev-Ye-Kitaev Model," 1705.03406. 4

[30] X.-Y. Song, C.-M. Jian, and L. Balents, "A strongly correlated metal built from Sachdev-Ye-Kitaev models," *arXiv preprint* (2017) 1705.00117. 4

[31] P. Zhang, "Dispersive SYK model: band structure and quantum chaos," 1707.09589. 4

[32] A. Haldar, S. Banerjee, and V. B. Shenoy, "Higher-dimensional SYK Non-Fermi Liquids at Lifshitz transitions," *ArXiv e-prints* (Oct., 2017) 1710.00842. 4

[33] M. Berkooz, P. Narayan, M. Rozali, and J. Simn, "Higher Dimensional Generalizations of the SYK Model," *JHEP* **01** (2017) 138, 1610.02422. 4

[34] G. Turiaci and H. Verlinde, "Towards a 2d QFT Analog of the SYK Model," *JHEP* **10** (2017) 167, 1701.00528. 4

[35] M. Berkooz, P. Narayan, M. Rozali, and J. Simn, "Comments on the Random Thirring Model," *JHEP* **09** (2017) 057, 1702.05105. 4

[36] C.-M. Jian, Z. Bi, and C. Xu, "A model for continuous thermal Metal to Insulator Transition," *Phys. Rev.* **B96** (2017), no. 11 115122, 1703.07793. 4

[37] Y. Gu, A. Lucas, and X.-L. Qi, "Energy diffusion and the butterfly effect in inhomogeneous Sachdev-Ye-Kitaev chains," *SciPost Phys.* **2** (2017), no. 3 018, 1702.08462. 4

[38] D. V. Khveshchenko, "Thickening and sickening the SYK model," 1705.03956. 4

[39] J. Murugan, D. Stanford, and E. Witten, "More on Supersymmetric and 2d Analogs of the SYK Model," *JHEP* **08** (2017) 146, 1706.05362. 4

[40] S.-K. Jian, Z.-Y. Xian, and H. Yao, "Quantum criticality and duality in the SYK/AdS$_2$ chain," 1709.02810. 4

[41] T. Faulkner, N. Iqbal, H. Liu, J. McGreevy, and D. Vegh, "From black holes to strange metals," 1003.1728. 8

[42] T. Faulkner, N. Iqbal, H. Liu, J. McGreevy, and D. Vegh, "Charge transport by holographic Fermi surfaces," *Phys. Rev.* **D88** (2013) 045016, 1306.6396. 8

[43] A. Mukhopadhyay and G. Policastro, "Phenomenological Characterization of Semiholographic Non-Fermi Liquids," *Phys. Rev. Lett.* **111** (2013), no. 22 221602, 1306.3941. 8

[44] B. Doucot, C. Ecker, A. Mukhopadhyay, and G. Policastro, "Density response and collective modes of semi-holographic non-Fermi liquids," 1706.04975. 8

[45] I. Affleck, "Quantum impurity problems in condensed matter physics," *Les Houches 2008 proceedings* (2008) 0809.3474. 9, 11

[46] A. Bray and M. Moore, "Replica theory of quantum spin glasses," *Journal of Physics C: Solid State Physics* **13** (1980), no. 24 L655. 10

[47] G. Refael and J. E. Moore, "Entanglement entropy of random quantum critical points in one dimension," *Physical review letters* **93** (2004), no. 26 260602, cond-mat/0406737. 13

[48] G. Refael and J. E. Moore, "Criticality and entanglement in random quantum systems," *Journal of physics a: mathematical and theoretical* **42** (2009), no. 50 504010, 0908.1986. 13

[49] A. B. Zamolodchikov, "Irreversibility of the Flux of the Renormalization Group in a 2D Field Theory," *JETP lett* **43** (1986), no. 12 730–732. 13

[50] R. Santachiara, "Increasing of entanglement entropy from pure to random quantum critical chains," *Journal of Statistical Mechanics: Theory and Experiment* **2006** (2006), no. 06 L06002, cond-mat/0602527. 13

[51] B. Swingle, "Entanglement does not generally decrease under renormalization," *Journal of Statistical Mechanics: Theory and Experiment* **2014** (2014), no. 10 P10041. 13

[52] T. Grover, "Certain General Constraints on the Many-Body Localization Transition," *ArXiv e-prints* (May, 2014) 1405.1471. 14

[53] R. A. Davison, W. Fu, A. Georges, Y. Gu, K. Jensen, and S. Sachdev, "Thermoelectric transport in disordered metals without quasiparticles: The Sachdev-Ye-Kitaev models and holography," *Phys. Rev.* **B95** (2017), no. 15 155131, 1612.00849. 14, 15

[54] J. Cardy, *Scaling and renormalization in statistical physics*, vol. 5. Cambridge university press, 1996. 14

[55] S. R. White, "Density matrix formulation for quantum renormalization groups," *Physical review letters* **69** (1992), no. 19 2863. 16

[56] U. Schollwöck, "The density-matrix renormalization group in the age of matrix product states," *Annals of Physics* **326** (2011), no. 1 96–192, 1008.3477. 16

[57] P. Calabrese and J. Cardy, "Entanglement entropy and conformal field theory," *J.Phys.* **A42** (2009) 504005, 0905.4013. 17

[58] A. M. Goldsborough and G. Evenbly, "Entanglement renormalization for disordered systems," 1708.07652. 19, 23

[59] C. Holzhey, F. Larsen, and F. Wilczek, "Geometric and renormalized entropy in conformal field theory," *Nucl. Phys.* **B424** (1994) 443–467, hep-th/9403108. 19

[60] V. Korepin, "Universality of entropy scaling in one dimensional gapless models," *Physical review letters* **92** (2004), no. 9 096402. 19

[61] P. Calabrese and J. Cardy, "Entanglement entropy and quantum field theory," *Journal of Statistical Mechanics: Theory and Experiment* **2004** (2004), no. 06 P06002. 19

[62] I. Peschel, "Calculation of reduced density matrices from correlation functions," *Journal of Physics A: Mathematical and General* **36** (2003), no. 14 L205. 20

[63] V. Berezinskii, "Kinetics of a quantum particle in a one-dimensional random potential," *WORLD SCIENTIFIC SERIES IN 20TH CENTURY PHYSICS* **11** (1995) 87–94. 21

[64] R. Pordes, D. Petravick, B. Kramer, D. Olson, M. Livny, A. Roy, P. Avery, K. Blackburn, T. Wenaus, F. Würthwein, *et. al.*, "The open science grid," in *Journal of Physics: Conference Series*, vol. 78, p. 012057, IOP Publishing, 2007. 28

[65] I. Sfiligoi, D. C. Bradley, B. Holzman, P. Mhashilkar, S. Padhi, and F. Wurthwein, "The pilot way to grid resources using glideinWMS," in *Computer Science and Information Engineering, 2009 WRI World Congress on*, vol. 2, pp. 428–432, IEEE, 2009. 28